EUROPEAN ORGANIZATION FOR NUCLEAR RESEARCH

L3 Note 2584
July 11, 2000

# Single and Multi-Photon Events with Missing Energy in $e^+e^-$ Collisions at $\sqrt{s} = 192$–$202$ GeV

The L3 Collaboration

## Abstract

Single and multi-photon events with missing energy are analysed using data collected with the L3 detector at LEP at centre-of-mass energies between 192 GeV and 202 GeV, for a total of 231.5 $pb^{-1}$ of integrated luminosity. The total cross section of the process $e^+e^- \to \nu\bar{\nu}\gamma(\gamma)$ is found in agreement with the Standard Model. Deviations are observed as far as the differential cross section is concerned. The multi-photon channel is in agreement with the Standard Model expectation both in the rate and in the two-photon recoil mass distribution. Preliminary upper limits on cross sections of supersymmetric processes are set using both single and multi-photon channels and interpretations in supersymmetric models provide improved limits on the masses of the lightest neutralino.

Submitted to the *XXXth International Conference on High Energy Physics*
July 27 - August 2, 2000, Osaka, Japan

# 1 Introduction

In the Standard Model [1] single or multi-photon events with missing energy are produced via the reaction $e^+e^- \to \nu\bar{\nu}\gamma(\gamma)$ which proceeds through $s$–channel Z exchange and $t$–channel W exchange. This note reports on searches for single and multi-photon final states and it follows the analysis procedures described in [2].

In supersymmetric models [3] different supersymmetry (SUSY) breaking mechanisms lead to different phenomenologies. The SUSY breaking scale, $\sqrt{F}$, or equivalently the gravitino mass ($m_{\tilde{\mathrm{G}}} = F/[\sqrt{3/(8\pi)}\, m_{\mathrm{P}}]$ where $m_{\mathrm{P}}$ is the Planck mass), is considered as a free parameter. Three different scenarios are distinguished: heavy, light and superlight gravitinos.

In gravity-mediated SUSY breaking models (SUGRA) the gravitino is heavy (100 GeV $\lesssim m_{\tilde{\mathrm{G}}} \lesssim$ 1 TeV) and thus does not play a role in production or decay processes. The lightest neutralino is the lightest supersymmetric particle (LSP), which is stable under the assumption of R–parity [4] conservation and escapes detection due to its weakly interacting nature. In this scenario, single or multi-photon signatures arise from pair-production of neutralinos ($\tilde{\chi}^0_1\tilde{\chi}^0_2$ and $\tilde{\chi}^0_2\tilde{\chi}^0_2$) [5]. Subsequent one-loop decays of $\tilde{\chi}^0_2$ into $\tilde{\chi}^0_1\gamma$ have a branching fraction close to 100% if one of the two neutralinos is pure photino and the other pure higgsino [6]. In general, neutralinos are mixtures of photinos, zinos and higgsinos.

In models with Gauge-Mediated SUSY Breaking (GMSB) [7], a light gravitino ($10^{-2}$ eV $\lesssim m_{\tilde{\mathrm{G}}} \lesssim 10^2$ eV) is the LSP. In this case the gravitino plays a fundamental role in the decay of SUSY particles. In particular, the $\tilde{\chi}^0_1$ is no longer stable and decays through $\tilde{\chi}^0_1 \to \tilde{\mathrm{G}}\gamma$ if it is the next-to lightest supersymmetric particle (NLSP) [8]. Pair-production of the lightest neutralino leads to a two-photon plus missing energy signature in the detector.

When the scale of local supersymmetry breaking is decoupled from the breaking of global supersymmetry as in no-scale supergravity models [9], the gravitino can be superlight ($10^{-6}$ eV $\lesssim m_{\tilde{\mathrm{G}}} \lesssim 10^{-4}$ eV). Then, it is produced not only in SUSY particle decays but also directly in pairs [10] or associated with a neutralino [11]. Pair-production of gravitinos accompanied by initial state radiation leads to a single photon signature. This signature also arises in $\tilde{\chi}^0_1\tilde{\mathrm{G}}$ production when the neutralino decays radiatively to gravitino and photon.

# 2 Data Sample and Simulation

In this analysis we use the data collected by the L3 detector [12] during the high energy run of LEP in 1999 corresponding to an integrated luminosity of 231.5 pb$^{-1}$ at the following four average centre-of-mass energies: 191.60 (hereafter called 192) GeV, 195.54 (196) GeV, 199.54 (200) GeV and 201.75 (202) GeV. All results given in the paper are preliminary.

Monte Carlo events for the following Standard Model processes are simulated: $e^+e^- \to \nu\bar{\nu}\gamma(\gamma)$ with `KORALZ` [13], $e^+e^- \to \gamma\gamma(\gamma)$ with `GGG` [14], Bhabha scattering for large scattering angles with `BHWIDE` [15], and for small scattering angles with `TEEGG` [16], and four-fermion final states specifically the processes $e^+e^- \to e^+e^-e^+e^-$ with `DIAG36` [17], and $e^+e^- \to e^+e^-\nu\bar{\nu}$ with `EXCALIBUR` [18].

SUSY processes are simulated with the Monte Carlo program `SUSYGEN` [19] for SUSY particle masses ($m_{\mathrm{SUSY}}$) between zero and the kinematic limit and, in $\tilde{\chi}^0_1$ LSP scenarios, for $\Delta m = m_{\mathrm{SUSY}} - m_{\mathrm{LSP}}$ between 1 GeV and $m_{\mathrm{SUSY}}$. To ensure the radiative decay of the neutralino, the scalar electron ($\tilde{e}_R$) mass is set to 110 GeV, except for $\tilde{\chi}^0_1\tilde{\mathrm{G}}$ production where it is set to 200 GeV. The detector response is simulated using the `GEANT` program [20], which takes into account the effects of energy loss, multiple scattering and showering in the detector.

# 3 Event Selection

Electrons and photons are measured accurately by the BGO electromagnetic calorimeter. They are required to have an energy greater than 0.9 GeV. The shape of their energy deposition must be consistent with an electromagnetic shower. Electrons are defined as electromagnetic clusters matched with a charged track reconstructed in the central tracking chamber. Identified conversion electrons from photons interacting with the beam pipe or with the silicon microvertex detector, 4% of the total, are also accepted as photons. Bhabha events and $e^+e^- \rightarrow \gamma\gamma(\gamma)$ events that are fully contained in the calorimeter are used to check the particle identification as well as the energy resolution, which is 1% for high energy electrons and photons in both the barrel and the endcaps. The barrel region is defined as the polar angle range $43^\circ < \theta < 137^\circ$ with respect to the beam axis and the endcap region as the polar angle range $14^\circ < \theta < 36^\circ$ or $144^\circ < \theta < 166^\circ$.

## 3.1 High Energy Photons

The selection of high energy single and multi-photon events requires at least one photon with energy greater than 5 GeV in the barrel or endcaps region. There must be no charged tracks apart from those consistent with photon conversion. The following cuts are imposed to suppress events which do not consist of photons only in the final state. The energy not assigned to identified photons has to be smaller than 10 GeV and the energy measured in the electromagnetic calorimeter between BGO barrel and endcaps must be smaller than 7 GeV. There must be no track in the muon chambers and at most one BGO cluster not identified as a photon.

To reduce the background from radiative Bhabha events with particles escaping along the beam pipe, as well as from the process $e^+e^- \rightarrow \gamma\gamma(\gamma)$, events with less than 20 GeV transverse momentum are rejected if energy is observed in the small polar angle detectors covering an angular range of $1.5^\circ - 10^\circ$. The total transverse momentum of photons is required to be greater than 5 GeV if no second photon with energy greater than 5 GeV is found. If two calorimetric clusters are present and if only one is identified as a photon, their acollinearity must be greater than $5.2^\circ$ and their acoplanarity must be greater than $2.4^\circ$. Furthermore, if a photon is detected with an acoplanarity less than $15^\circ$ to a hadron calorimeter (HCAL) cluster the energy of that cluster must be less than 3 GeV.

When a second photon with energy above 5 GeV is present, the total transverse momentum must be greater than 3 GeV and the recoil mass must be larger than 20 GeV. If the total transverse momentum is smaller than 30 GeV, the acollinearity is required to be larger than $8.1^\circ$ and the acoplanarity to be larger than $5.2^\circ$. If the transverse momentum is smaller than 20 GeV, the missing momentum direction is required to be at least $7^\circ$ away from the beam pipe. If the acoplanarity is smaller than $2.4^\circ$, the recoil mass must be greater than 50 GeV.

To suppress cosmic ray background, we require for photon energies smaller than 15 GeV, that the most energetic photon is not aligned with hits in the muon detector. For photon energies larger than 15 GeV, there must be at least one scintillator time measurement within $\pm 5$ ns of the beam crossing time. Furthermore, an event is rejected if more than 20 hits are found in the central tracking chamber in a 1 cm road between any pair of energy depositions in the BGO. The cosmic ray background in the event sample is estimated from studies of out-of-time events. The overall efficiency for $e^+e^- \to \nu\bar{\nu}\gamma(\gamma)$ events satisfying the kinematic requirements $E_\gamma > 5$ GeV and $|\cos\theta_\gamma| < 0.97$ is about 58.6%.

The number of events with one or more photons selected at different centre-of-mass energies together with the Monte Carlo expectation, measured and expected cross section is listed in Table 1. The systematic error on the cross section is composed of the errors on the corrections due to detector noise and photon identification, an uncertainty on the amount of converted photons and an error due to limited Monte Carlo statistics. Figure 1 shows the energy spectra of the most energetic photon normalised to the beam energy for single and multi-photon events.

The absolute rate is in excellent agreement with the Monte Carlo prediction. On the contrary, the photon energy distribution and to a lesser extent the polar angle distribution show discrepancies with respect to the Monte Carlo prediction, as can be seen from Table 2. These discrepancies have been subject to extensive investigations concerning the performance of sub-detectors and triggers used in this analysis. The noise level of sub-detectors is studied using randomly triggered beam-gate events. The performance of the electromagnetic calorimeter is cross-checked with full-energy and radiative Bhabha events. Triggers important for single and multi-photon events are investigated using single electron[1)] and Bhabha events. The theoretical predictions for the differential cross section of $e^+e^- \to \nu\bar{\nu}\gamma\gamma(\gamma)$ obtained from `KORALZ`, `NUNUGPV` [21] and `GRACE` [22] are found to agree within 5%. No systematic effect is found to explain the discrepancies in the photon energy distribution. An independent analysis leads to the same conclusion, as it can be seen from Figure 2. Figure 3 shows both the $\nu\bar{\nu}\gamma(\gamma)$ cross section measurement and the total neutrino-pair extrapolation versus centre-of-mass energy together with the prediction of the Standard Model and measurements at lower centre-of-mass energies.

For the sub-sample of events with two or more photons a minimum energy for the second photon of 1 GeV is required. In the data 49 events are observed compared to a Monte Carlo prediction of 40.6 events. Figure 4 shows the two-photon recoil mass distribution. The lack of multi-photon events observed at 189 GeV is not confirmed [2].

# 4 Neutrino Counting

To determine the number of light neutrino species a maximum likelihood fit to the photon energy spectra is performed at each centre-of-mass energy above the Z resonance. For each energy interval the theoretical prediction is obtained by linearly interpolating `KORALZ` predictions for $N_\nu = 1, 2, 3, 4, 5$. Due to the different contributions to the energy spectrum from $\nu_e\bar{\nu}_e$ $t$–channel production via W exchange and $\nu\bar{\nu}$ $s$–channel production via Z exchange, this method is more powerful than using the total cross section measurement. Figure 5 shows the energy spectra of the most energetic photon normalised to the beam energy for the events selected at 192-202 GeV compared to the expectation with $N_\nu = 2$ and $N_\nu = 4$. In addition to the systematic error from the cross section measurement, the theoretical uncertainty on the photon energy spectrum – estimated by comparing `KORALZ` with `NUNUGPV` – is taken into account. The main contributions to the overall systematic error are coming from the theoretical uncertainty and an error due to limited Monte Carlo statistics. The result is $N_\nu = 2.77 \pm 0.14 \pm 0.08$.

Combining this result with our previous measurement at $\sqrt{s}$= 189 GeV gives:

$$N_\nu = 2.86 \pm 0.10 \pm 0.08\,.$$

[1)] Radiative Bhabha scattering events where one electron and a photon have a very low polar angle, and only a low energetic electron is scattered with a large polar angle.

# 5 Limits on New Physics

The limits derived in the following are obtained from 192-202 GeV data combined with our previous results at 189 GeV [2]. They correspond to a confidence level of 95%. Cross section limits are calculated using a likelihood approach [23] where the spectra of a discriminant variable for data, background and signal simulations are compared.

## 5.1 Single Photon Signature

The reaction $e^+e^- \rightarrow \tilde{G}\tilde{\chi}^0_1$ proceeds through $s$–channel Z exchange and $t$–channel $\tilde{e}_{L,R}$ exchange. Efficiencies for this process with $\tilde{\chi}^0_1 \rightarrow \tilde{G}\gamma$ range between about 60% for $m_{\tilde{\chi}^0_1} = 0.5$ GeV and 70% for $m_{\tilde{\chi}^0_1}$ at the kinematic limit. Here, the discriminant variable used to derive cross section limits is the photon energy. The cross section upper limit at $\sqrt{s} = 202$ GeV as a function of $m_{\tilde{\chi}^0_1}$ is shown in Figure 6a) together with the expected limit obtained in Monte Carlo trials with background only, data collected at lower centre-of-mass energies are included assuming the signal cross section to scale as $1/s$. The no-scale SUGRA model of [11], referred to as LNZ, has only two free parameters – gravitino and neutralino masses. The neutralino is the NLSP, which is almost pure bino. Here, the dominant decay channel is $\tilde{\chi}^0_1 \rightarrow \tilde{G}\gamma$. The small contribution of the decay into Z for $m_{\tilde{\chi}^0_1} \gtrsim 100$ GeV is taken into account. Figure 6b) shows exclusion contours in the $m_{\tilde{G}} - m_{\tilde{\chi}^0_1}$ plane. Gravitino masses below $10^{-5}$ eV are excluded for neutralino masses below 168 GeV.

## 5.2 Multi-Photon Signature

Using a binned likelihood technique, the discriminant variable is constructed for the multi-photon events combining the energies of the two most energetic photons, their polar angles, recoil mass, and the polar angle of the missing momentum vector. For each event class, background and signal Monte Carlo processes, denoted by $j$, and each input quantity $i$, a probability density function $f^i_j$ is computed and the discriminant variable of an event is then given by

$$F(\vec{x}) = \frac{\prod_i p^i_{\mathrm{signal}}(x_i)}{\sum_j \prod_i p^i_j(x_i)} \quad \text{with} \quad p^i_j(x_i) = \frac{f^i_j(x_i)}{\sum_k f^i_k(x_i)} ,$$

where $x_i$ are the measured values of the six input variables of an event. The distribution of the discriminant is shown in Figure 7 for $\tilde{\chi}^0_1\tilde{\chi}^0_1 \rightarrow \tilde{G}\tilde{G}\gamma\gamma$ with $m_{\tilde{\chi}^0_1} = 97$ GeV.

In the heavy gravitino scenario, a two-photon signature is produced by the process $e^+e^- \rightarrow \tilde{\chi}^0_2\tilde{\chi}^0_2$ and subsequent decay to $\tilde{\chi}^0_1\gamma$. Typical efficiencies for this process are around 65%. Cross section upper limits at $\sqrt{s} = 202$ GeV are obtained as shown in Figure 8a), data collected at lower centre-of-mass energies are included assuming the signal cross section to scale as $\beta/s$.

The interpretation of the $ee\gamma\gamma$ event with large transverse missing energy observed by CDF [24] suggests a high branching ratio for the radiative decay of the $\tilde{\chi}^0_2$ in the heavy gravitino scenario, which can be achieved if $\tilde{\chi}^0_2$ is a pure photino and $\tilde{\chi}^0_1$ is a pure higgsino. With this assumption, the lower mass limit of $\tilde{\chi}^0_2$ as a function of the scalar electron mass is calculated for mass differences between $\tilde{\chi}^0_2$ and $\tilde{\chi}^0_1$ greater than 10 GeV as shown in Figure 8b). For each $\tilde{\chi}^0_2$ mass, the exclusion is obtained using the most conservative cross section upper limit for any $\Delta m > 10$ GeV. The regions kinematically allowed [25] for the CDF event are overlayed in Figure 8b). The two exclusions obtained for equal masses of $\tilde{e}_{L,R}$ and for $m_{\tilde{e}_L} \gg m_{\tilde{e}_R}$ are shown in the interesting mass range for $m_{\tilde{e}_R}$.

The selection described in this paper is devised for photons originating from the interaction point. For a neutralino mean decay length $d_{\tilde{\chi}_1^0}$ larger than 1 cm the experimental sensitivity drops. This problem arises only for peculiar situations in the light gravitino scenario. The following limits in the gravitino LSP scenario are derived under the assumption of $d_{\tilde{\chi}_1^0} < 1$ cm. The cross section limits at $\sqrt{s} = 202$ GeV for the process $\mathrm{e^+e^-} \rightarrow \tilde{\chi}_1^0\tilde{\chi}_1^0 \rightarrow \tilde{\mathrm{G}}\tilde{\mathrm{G}}\gamma\gamma$ are displayed in Figure 9a) versus neutralino mass, data collected at lower centre-of-mass energies are included assuming the signal cross section to scale as $\beta/s$.

The efficiency varies between 17% for $m_{\tilde{\chi}_1^0} = 0.5$ GeV and 63% for $m_{\tilde{\chi}_1^0} = 98$ GeV. Theoretical predictions for two extreme cases of neutralino content[2)] [26], which determines its coupling to the photon, are shown in the same Figure. For these two cases of neutralino content a lower limit of

$$m_{\tilde{\chi}_1^0} > 94.7 \text{ GeV},$$

is derived assuming a neutralino NLSP scenario. Figure 9b) shows the exclusion in the $\tilde{\chi}_1^0 - \tilde{\mathrm{e}}_{\mathrm{L,R}}$ mass plane derived with our data for a neutralino being pure bino. The $\mathrm{ee}\gamma\gamma$ event observed by CDF also has an interpretation in supersymmetric models with gravitino LSP [26]. Our analysis almost rules out this interpretation as shown in Figure 9b).

# 6 Acknowledgements

We wish to express our gratitude to the CERN accelerator division for the excellent performance of the LEP machine. We acknowledge the effort of the engineers and technicians who have participated in the construction and maintenance of this experiment.

[2)]For the higgsino case a 2% photino component is required to ensure the decay into $\gamma\tilde{\mathrm{G}}$.

# References


[1] S.L. Glashow, Nucl. Phys. **22** (1961) 579;
S. Weinberg, Phys. Rev. Lett. **19** (1967) 1264;
A. Salam, *Elementary Particle Theory*, Ed. N. Svartholm, Stockholm, Almquist and Wiksell (1968), 367.

[2] L3 Collab., M. Acciarri *et al.*, *Single and Multi-Photon Events with Missing Energy in* $e^+e^-$ *collisions at* $\sqrt{s} = 189$ *GeV*, 1999, Phys. Lett. **B 470** (1999) 268.

[3] Y.A. Golfand and E.P. Likhtman, Sov. Phys. JETP **13** (1971) 323;
D.V. Volkhov and V.P. Akulov, Phys. Lett. **B 46** (1973) 109;
J. Wess and B. Zumino, Nucl. Phys. **B 70** (1974) 39;
P. Fayet and S. Ferrara, Phys. Rep. **C 32** (1977) 249;
A. Salam and J. Strathdee, Fortschr. Phys. **26** (1978) 57.

[4] P. Fayet, Nucl. Phys. **B 90** (1975) 104;
A. Salam and J. Strathdee, Nucl. Phys. **B 87** (1975) 85.

[5] A. Bartl, H. Fraas and W. Majerotto, Nucl. Phys. **B 278** (1986) 1;
S. Ambrosanio and B. Mele, Phys. Rev. **D 52** (1995) 3900.

[6] P. Fayet, Phys. Lett. **B 117** (1982) 460;
H.E. Haber and D. Wyler, Nucl. Phys. **B 323** (1989) 267;
S. Ambrosanio and B. Mele, Phys. Rev. **D 53** (1996) 2541;
S. Ambrosanio *et al.*, Phys. Rev. Lett. **76** (1996) 3498.

[7] M. Dine and A.E. Nelson, Phys. Rev. **D 48** (1993) 1277;
M. Dine, A.E. Nelson and Y. Shirman, Phys. Rev. **D 51** (1995) 1362;
M. Dine, A.E. Nelson, Y. Nir and Y. Shirman, Phys. Rev. **D 53** (1996) 2658.

[8] J. Ellis and J.S. Hagelin, Phys. Lett. **B 122** (1983) 303;
J. Ellis *et al.*, Phys. Lett. **B 147** (1984) 99;
P. Fayet, Phys. Lett. **B 175** (1986) 471;
S. Dimopoulos *et al.*, Phys. Rev. Lett. **76** (1996) 3494;
D.R. Stump *et al.*, Phys. Rev. **D 54** (1996) 1936.

[9] E. Cremmer, S. Ferrara, C. Kounnas and D.V. Nanopoulos, Phys. Lett. **B 133** (1983) 61;
J. Ellis, A. Lahanas, D.V. Nanopoulos and K. Tamvakis, Phys. Lett. **B 134** (1984) 429;
J. Ellis, C. Kounnas and D.V. Nanopoulos, Nucl. Phys. **B 241** (1984) 406;
J. Ellis, C. Kounnas and D.V. Nanopoulos, Nucl. Phys. **B 247** (1984) 373;
J. Ellis, K. Enqvist and D.V. Nanopoulos, Phys. Lett. **B 147** (1984) 99.

[10] A. Brignole, F. Feruglio and F. Zwirner, Nucl. Phys. **B 516** (1998) 13.

[11] J.L. Lopez, D.V. Nanopoulos and A. Zichichi, Phys. Rev. Lett. **77** (1996) 5168;
J.L. Lopez, D.V. Nanopoulos and A. Zichichi, Phys. Rev. **D 55** (1997) 5813.

[12] L3 Collab., B. Adeva *et al.*, Nucl. Instr. and Meth. **A 289** (1990) 35;
M. Chemarin *et al.*, Nucl. Instr. and Meth. **A 349** (1994) 345;
M. Acciarri *et al.*, Nucl. Instr. and Meth. **A 351** (1994) 300;

G. Basti *et al.*, Nucl. Instr. and Meth. **A 374** (1996) 293;
I.C. Brock *et al.*, Nucl. Instr. and Meth. **A 381** (1996) 236;
A. Adam *et al.*, Nucl. Instr. and Meth. **A 383** (1996) 342.

[13] The `KORALZ` version 4.03 is used.
S. Jadach, B.F.L. Ward and Z. Wąs, Comp. Phys. Comm. **79** (1994) 503.

[14] F.A. Berends and R. Kleiss, Nucl. Phys. **B 186** (1981) 22.

[15] S. Jadach *et al.*, Phys. Lett. **B 390** (1997) 298.

[16] The `TEEGG` version 7.1 is used.
D. Karlen, Nucl. Phys. **B 289** (1987) 23.

[17] F.A. Berends, P.H. Daverfeldt and R. Kleiss, Nucl. Phys. **B 253** (1985) 441.

[18] F.A. Berends, R. Pittau and R. Kleiss, Comp. Phys. Comm. **85** (1995) 437.

[19] S. Katsanevas and P. Morawitz, Comp. Phys. Comm. **112** (1998) 227.

[20] The L3 detector simulation is based on `GEANT` Version 3.15.
See R. Brun *et al.*, *GEANT 3*, CERN DD/EE/84-1 (Revised), September 1987.
The `GHEISHA` program (H. Fesefeldt, RWTH Aachen Report PITHA 85/02 (1985)) is used to simulate hadronic interactions.

[21] G. Montagna, M. Moretti, O. Nicrosini and F. Piccinini, Nucl. Phys. **B 541** (1999) 31.

[22] J. Fujimoto et. al., Comp. Phys. Comm. **100** (1997) 128.

[23] A. Favara and M. Pieri, *Confidence level estimation and analysis optimisation*, Preprint DFF-278/4/1997, E-preprint hep-ex 9706016.

[24] CDF Collab., F. Abe *et al.*, Phys. Rev. Lett. **81** (1998) 1791.

[25] S. Ambrosanio, G. Kane, G. Kribs, S. Martin and S. Mrenna, Phys. Rev. **D 55** (1996) 1372.

[26] J.L. Lopez and D.V. Nanopoulos, Phys. Rev. **D 55** (1997) 4450.

| $\sqrt{s}$ (GeV) | Luminosity ($pb^{-1}$) | $N_{data}$ | $N_{exp}$ | $\sigma_{measured}$(pb) | $\sigma_{exp}$(pb) |
|---|---|---|---|---|---|
| 192 | 29.5 | 85 | 87.9 | $4.89 \pm 0.53 \pm 0.08$ | 5.07 |
| 196 | 83.0 | 242 | 242.6 | $4.86 \pm 0.32 \pm 0.07$ | 4.87 |
| 200 | 82.1 | 225 | 236.0 | $4.60 \pm 0.31 \pm 0.08$ | 4.82 |
| 202 | 36.9 | 113 | 105.9 | $5.12 \pm 0.50 \pm 0.09$ | 4.79 |
| Total | 231.5 | 665 | 672.4 | | |

Table 1: The number of events with one or more photons selected at different centre-of-mass energies together with the Monte Carlo expectation, measured and expected cross section.

| Barrel | | |
|---|---|---|
| | Data | MC |
| $x < 0.65$ | 207 | 166.1 |
| $x > 0.65$ | 176 | 184.5 |
| Total | 383 | 350.6 |
| Endcaps | | |
| | Data | MC |
| $x < 0.65$ | 123 | 117.3 |
| $x > 0.65$ | 159 | 204.5 |
| Total | 282 | 321.8 |
| Combined | | |
| | Data | MC |
| $x < 0.65$ | 330 | 283.4 |
| $x > 0.65$ | 335 | 389.0 |
| Total | 665 | 672.4 |

Table 2: Number of events selected in data and Monte Carlo predictions in the indicated kinematic regions.

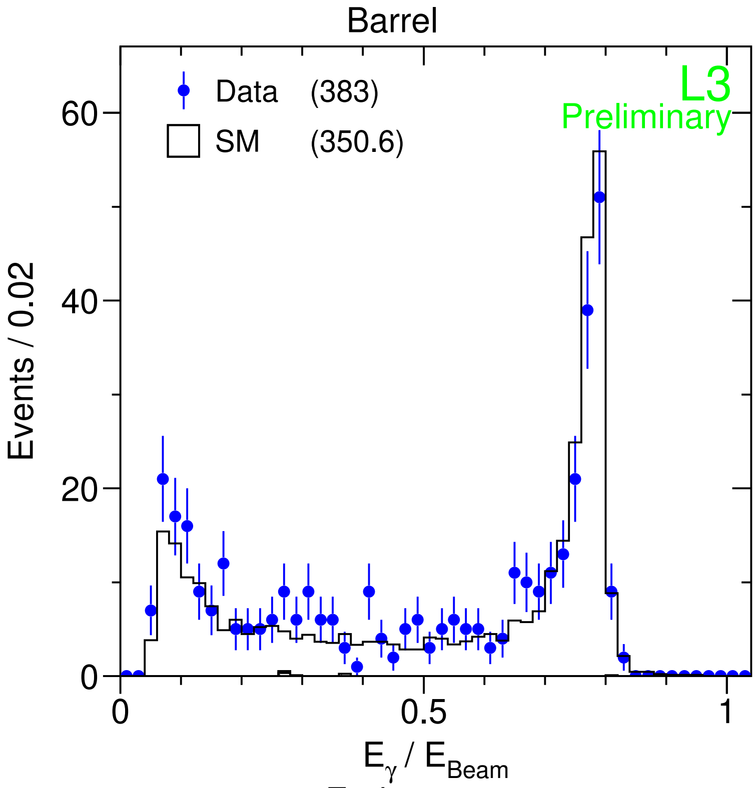


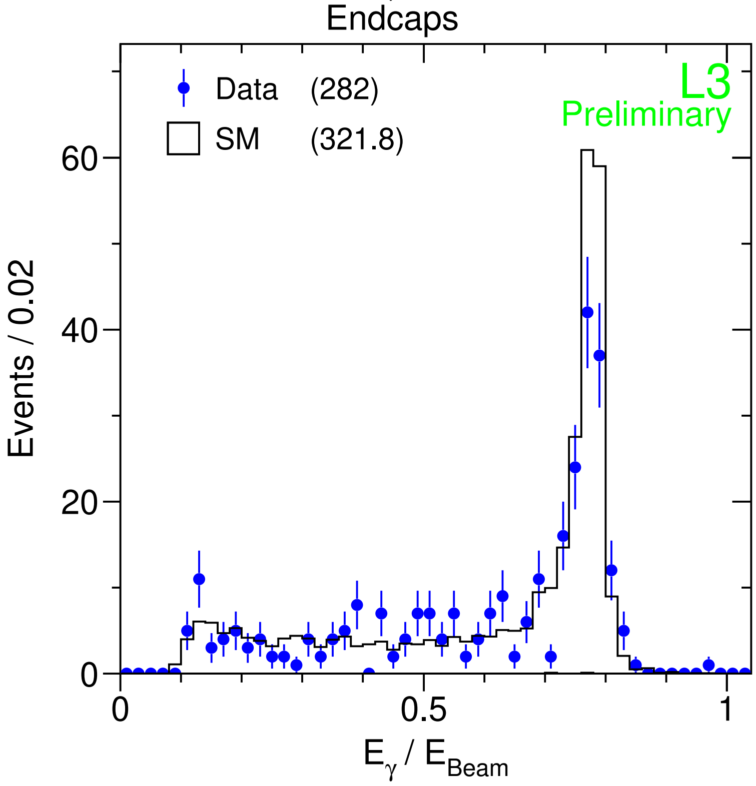


Figure 1: Energy of the highest energetic photon normalised to the beam energy for single and multi-photon events at 192-202 GeV in the barrel region (upper plot) and the same distribution for the endcap region.

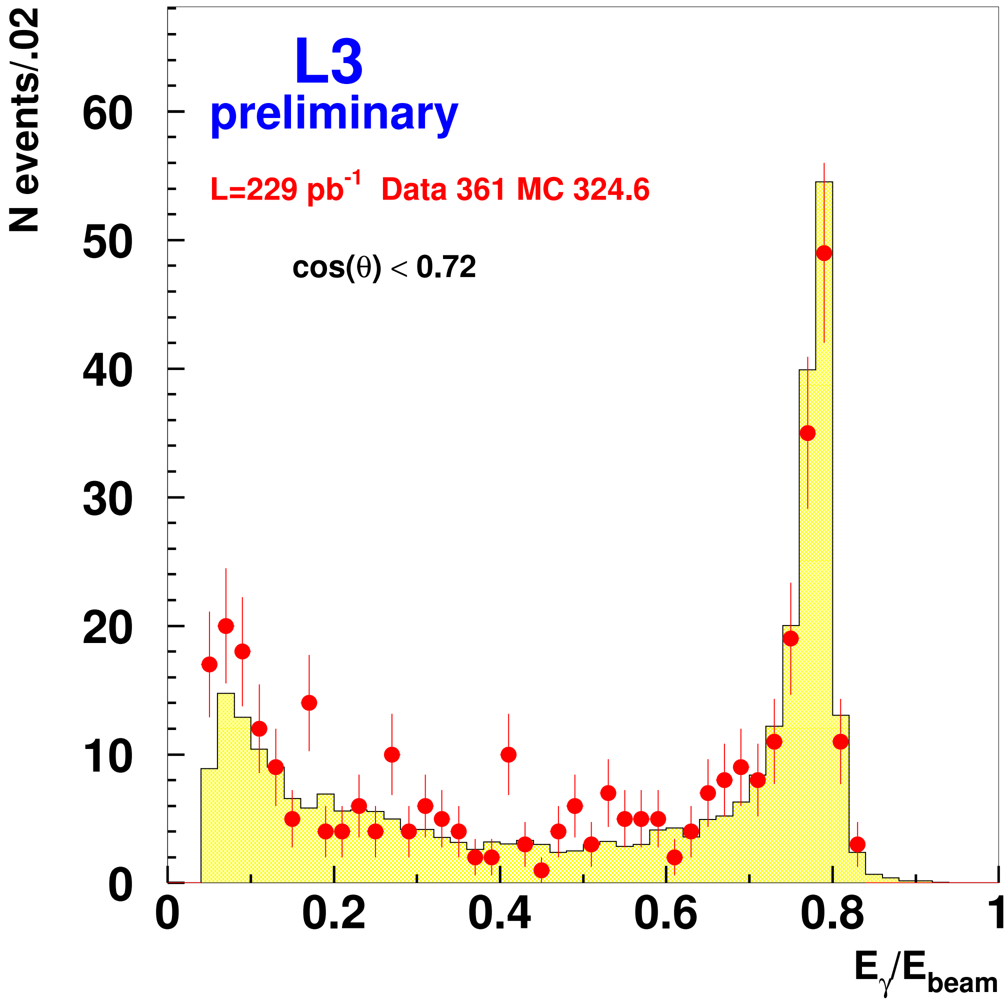


Figure 2: Energy of the highest energetic photon normalised to the beam energy for single and multi-photon events at 192-202 GeV in the barrel region as obtained by an independent analysis.

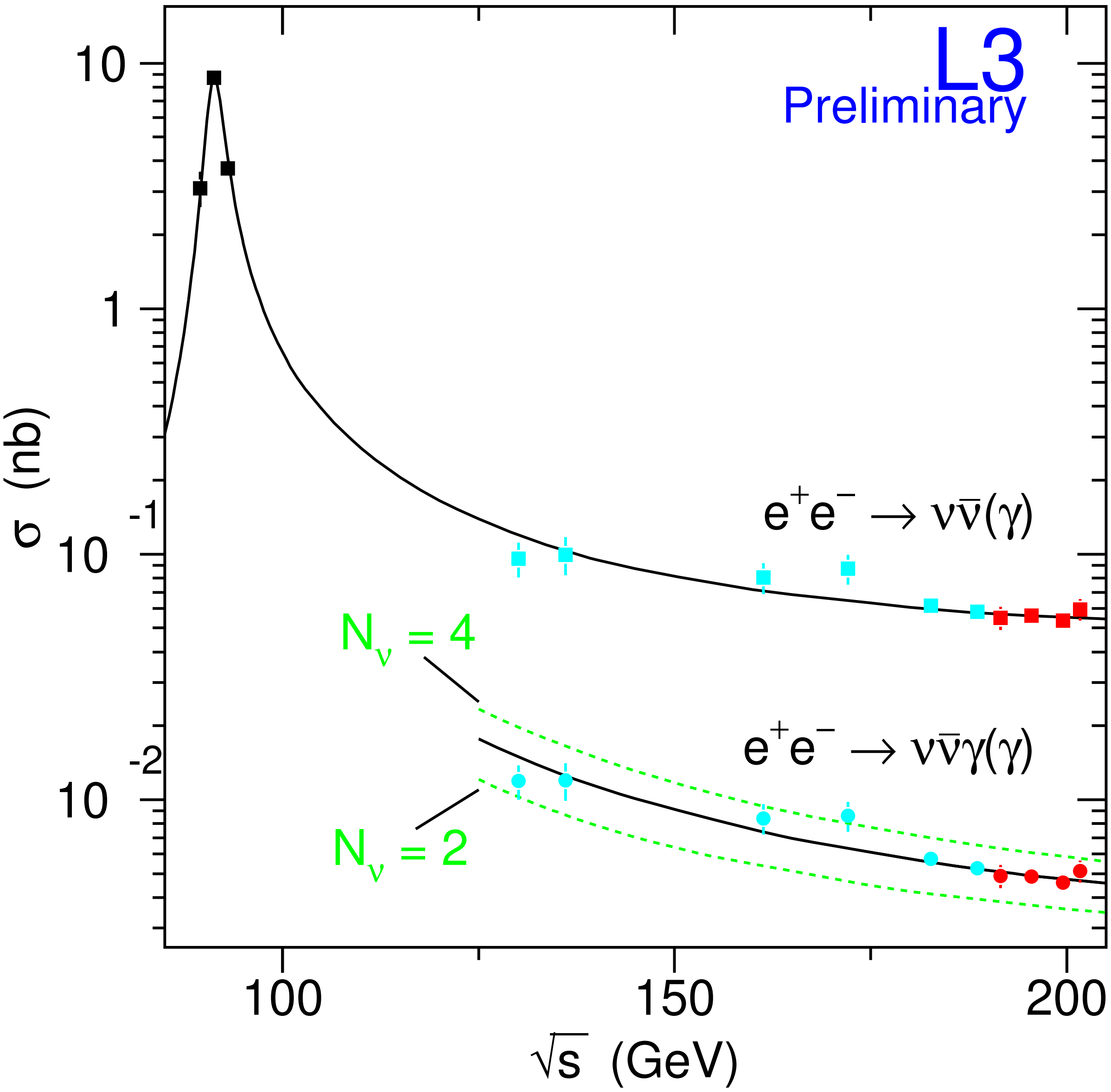


Figure 3: Production cross section of $\mathrm{e^+e^-} \rightarrow \nu\bar{\nu}(\gamma)$ and $\mathrm{e^+e^-} \rightarrow \nu\bar{\nu}\gamma(\gamma)$ as a function of the centre-of-mass energy. Points with error bars represent the $\nu\bar{\nu}\gamma(\gamma)$ measurements and squares with error bars are the extrapolation to $\nu\bar{\nu}(\gamma)$. The full line is the theoretical prediction for $N_\nu = 3$ and dashed lines are predictions for $N_\nu = 2, 4$ as indicated.

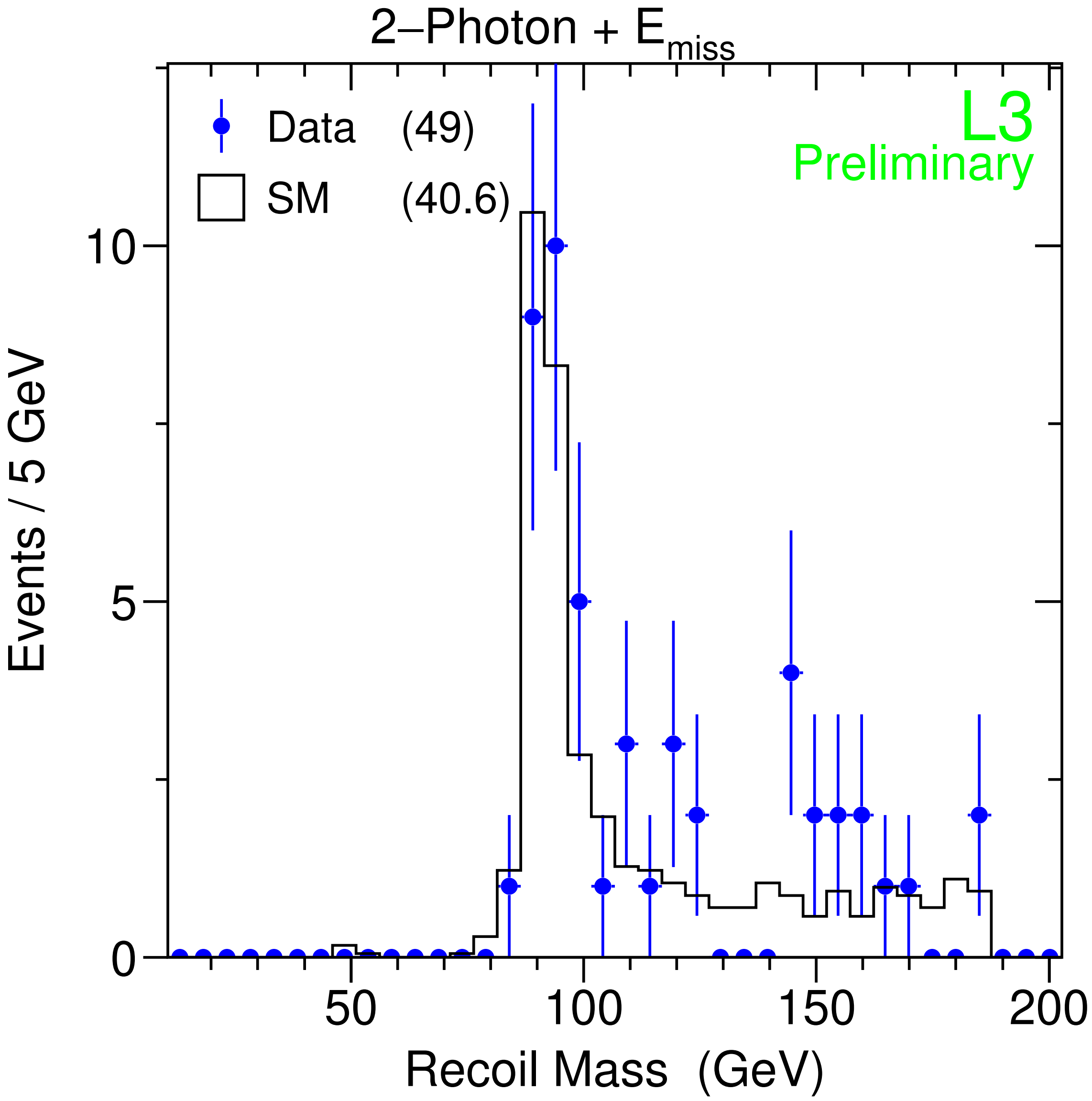


Figure 4: Recoil mass for the multi-photon sample collected at 192-202 GeV.

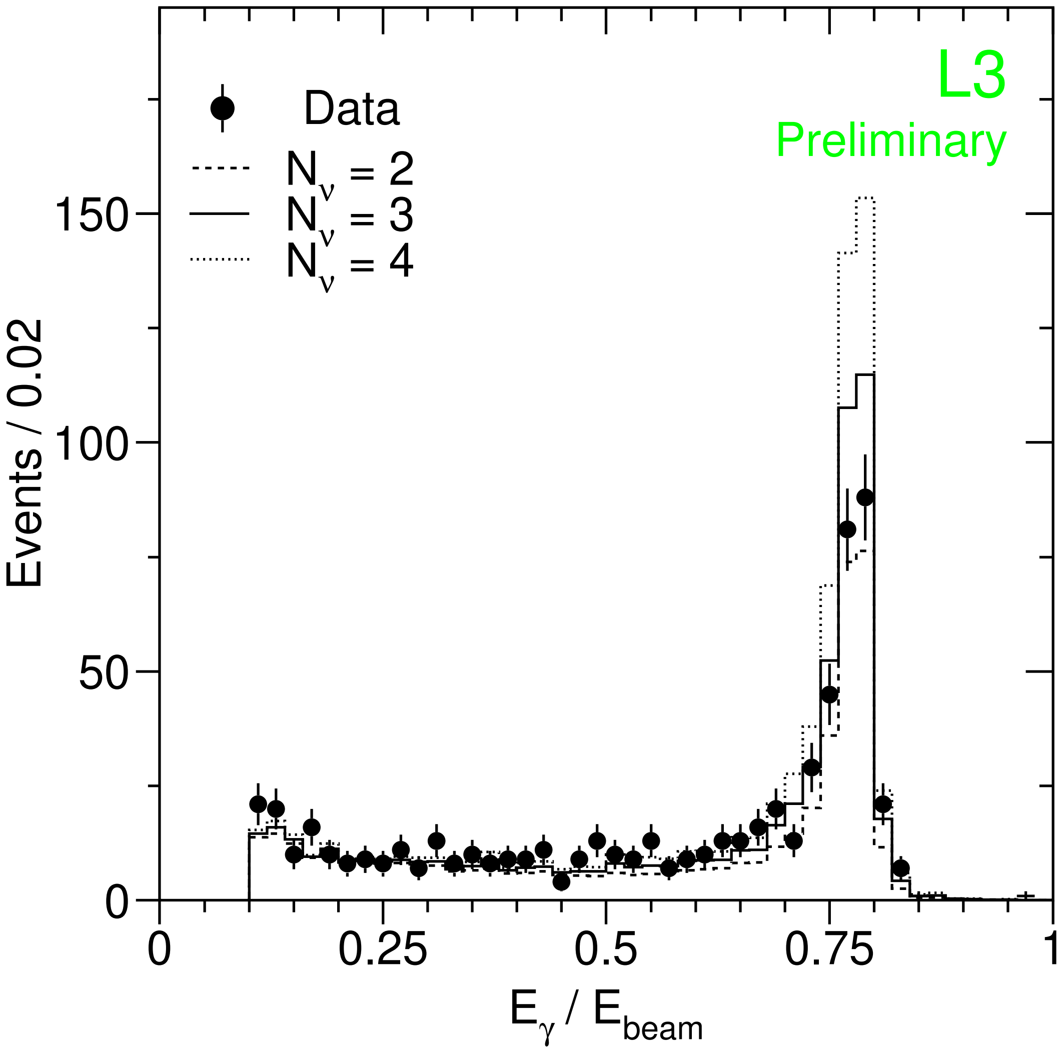


Figure 5: The energy spectra of the most energetic photon normalised to the beam energy for the events selected at 192-202 GeV compared to the expectation with $N_\nu = 2$ and $N_\nu = 4$.

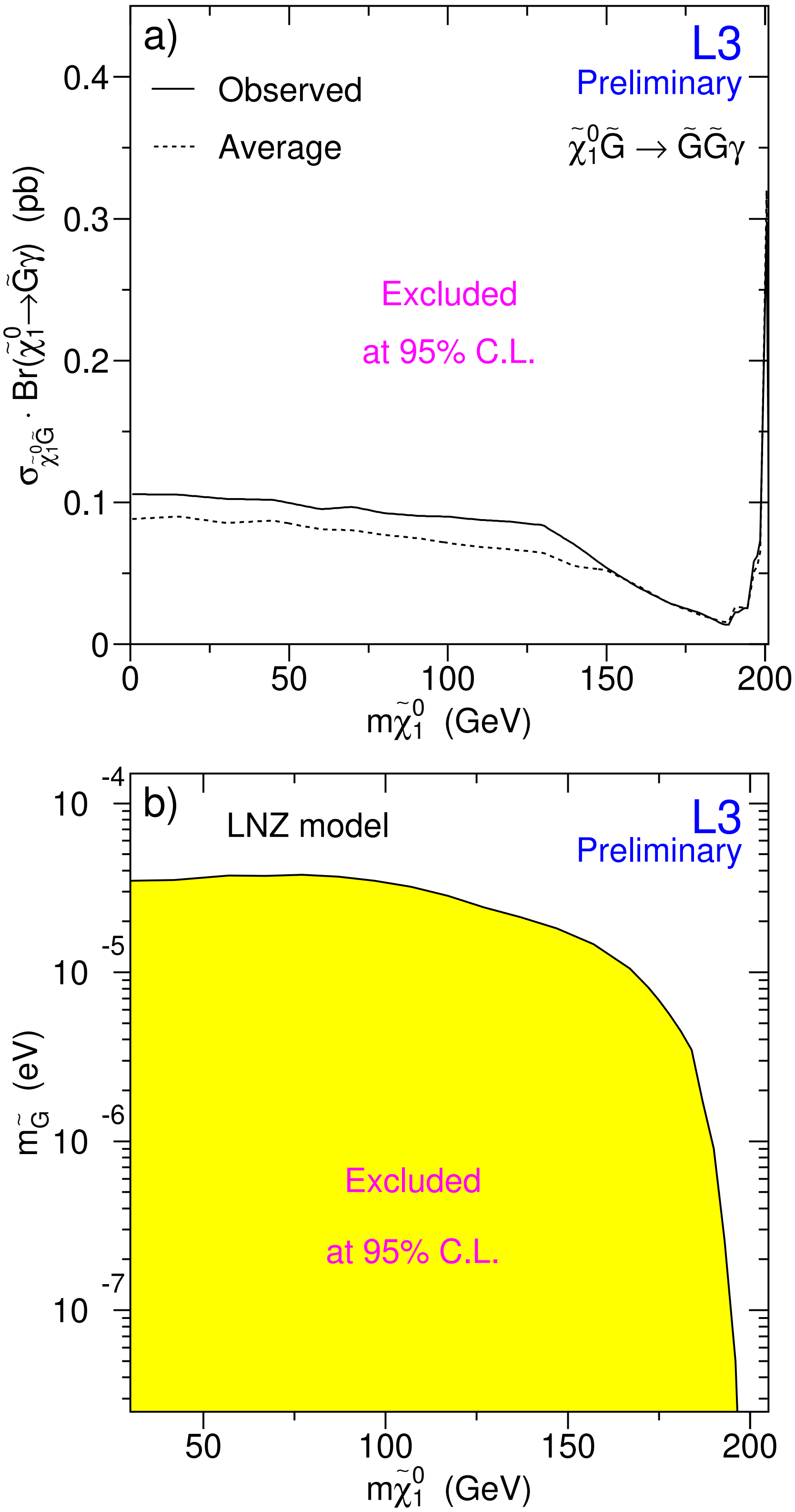


Figure 6: (a) Upper limit at $\sqrt{s} = 202$ GeV on the production cross section for the process $e^+e^- \to \tilde{G}\tilde{\chi}_1^0 \to \tilde{G}\tilde{G}\gamma$ and average limit obtained using Monte Carlo trials with background only, data collected at lower centre-of-mass energies are included assuming the signal cross section to scale as $1/s$. (b) Region excluded in the LNZ model in the plane $m_{\tilde{G}}$ versus $m_{\tilde{\chi}_1^0}$.

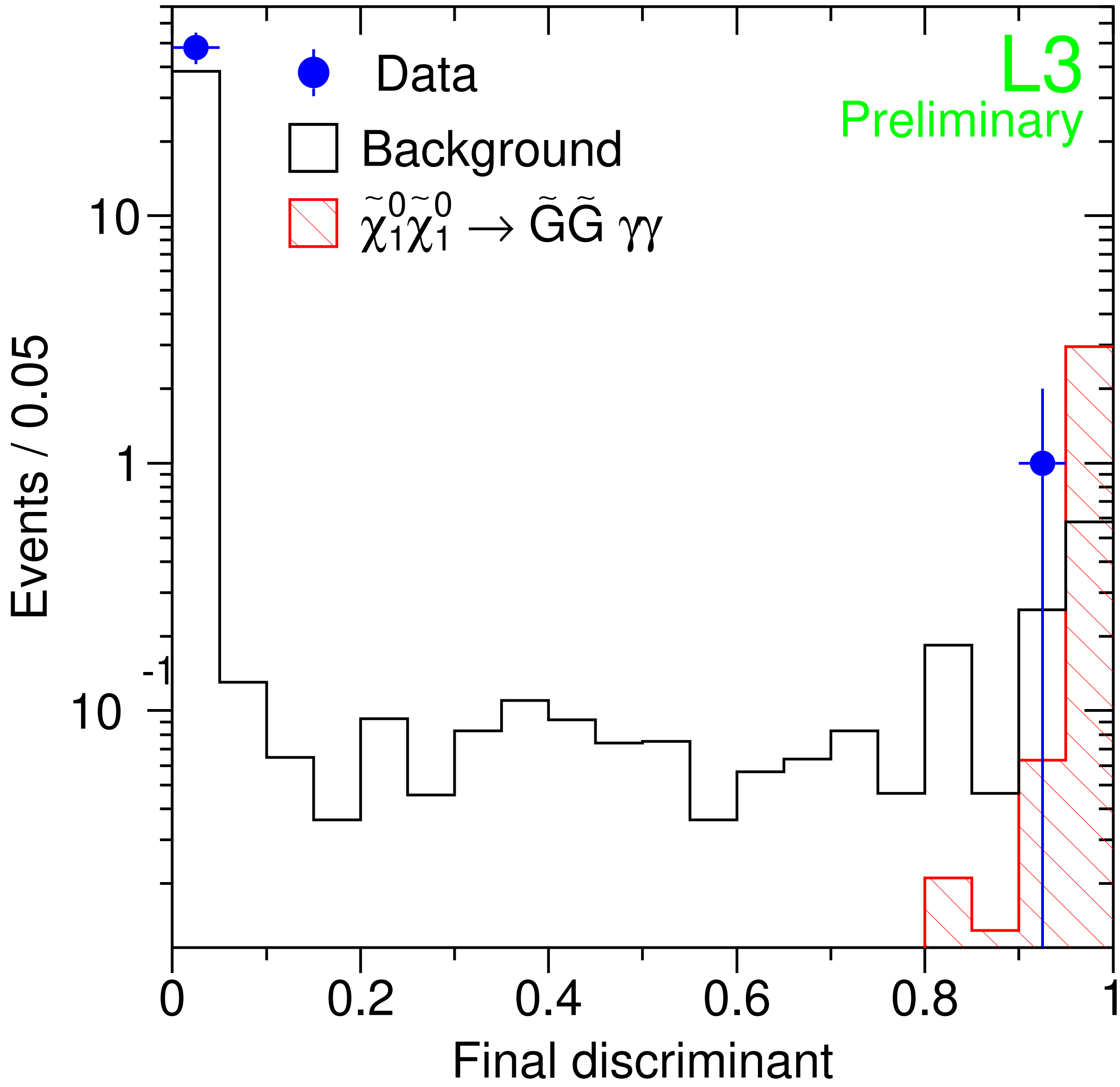


Figure 7: Discriminant variable for $\tilde{\chi}^0_1\tilde{\chi}^0_1 \to \tilde{G}\tilde{G}\gamma\gamma$ with $m_{\tilde{\chi}^0_1} = 97$ GeV for multi-photon events selected at 192-202 GeV. The signal corresponds to the upper limit of 3.12 events derived for this mass point.

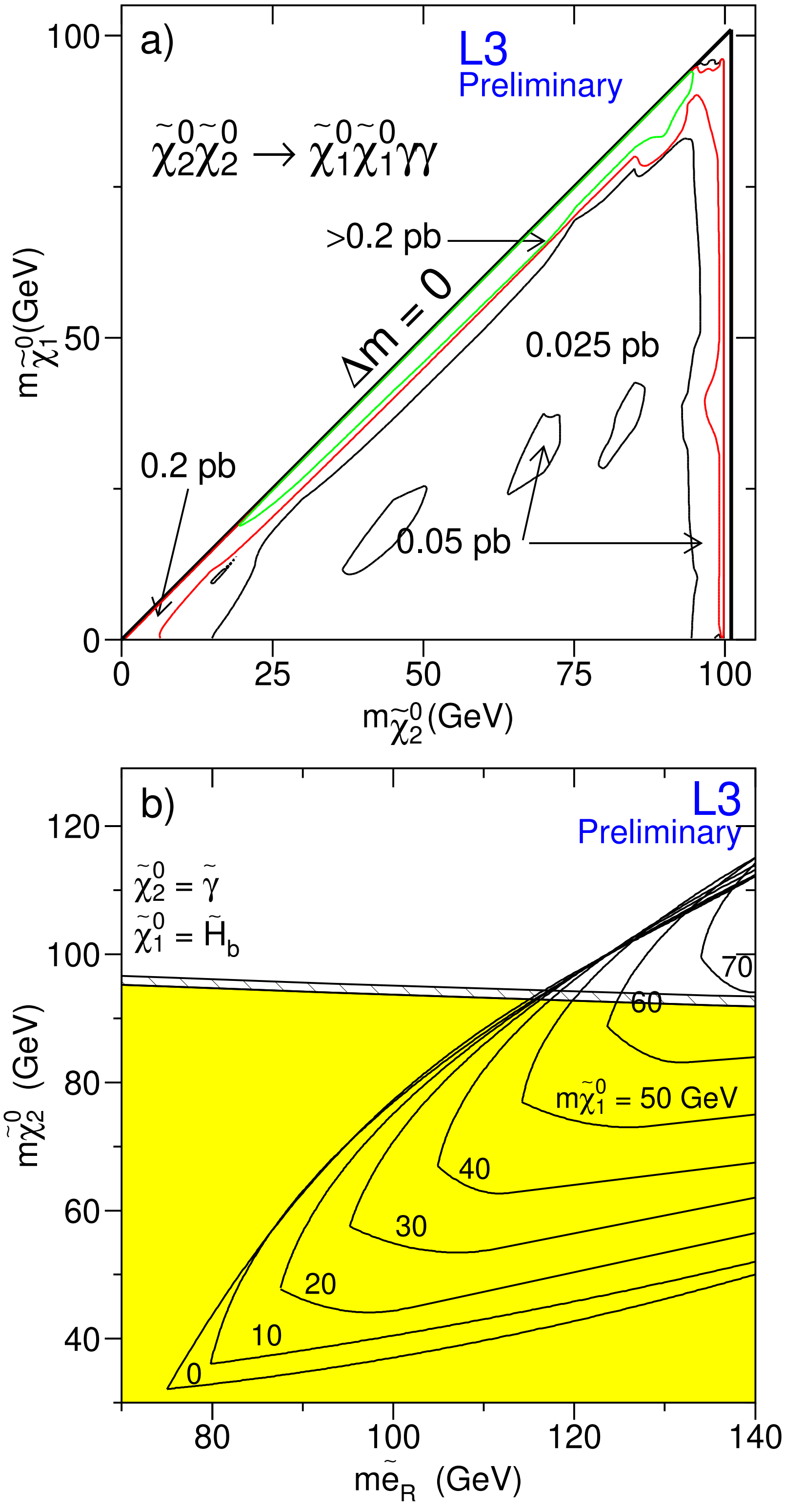


Figure 8: (a) Upper limits on the production cross section in picobarn for the process $e^+e^- \to \tilde{\chi}^0_2\tilde{\chi}^0_2 \to \tilde{\chi}^0_1\tilde{\chi}^0_1\gamma\gamma$ at $\sqrt{s} = 202$ GeV. Data collected at lower centre-of-mass energies are included assuming the signal cross section to scale as $\beta/s$. (b) Excluded region in the neutralino selectron mass plane. The shaded region corresponds to $m_{\tilde{e}_L} \gg m_{\tilde{e}_R}$ and the hatched region is additionally excluded when $m_{\tilde{e}_L} = m_{\tilde{e}_R}$. Regions kinematically allowed for the CDF event [25] as a function of $m_{\tilde{\chi}^0_1}$ are indicated, where $\tilde{\chi}^0_1 = \tilde{H}_b = \tilde{H}^0_1 \sin\beta + \tilde{H}^0_2 \cos\beta$.

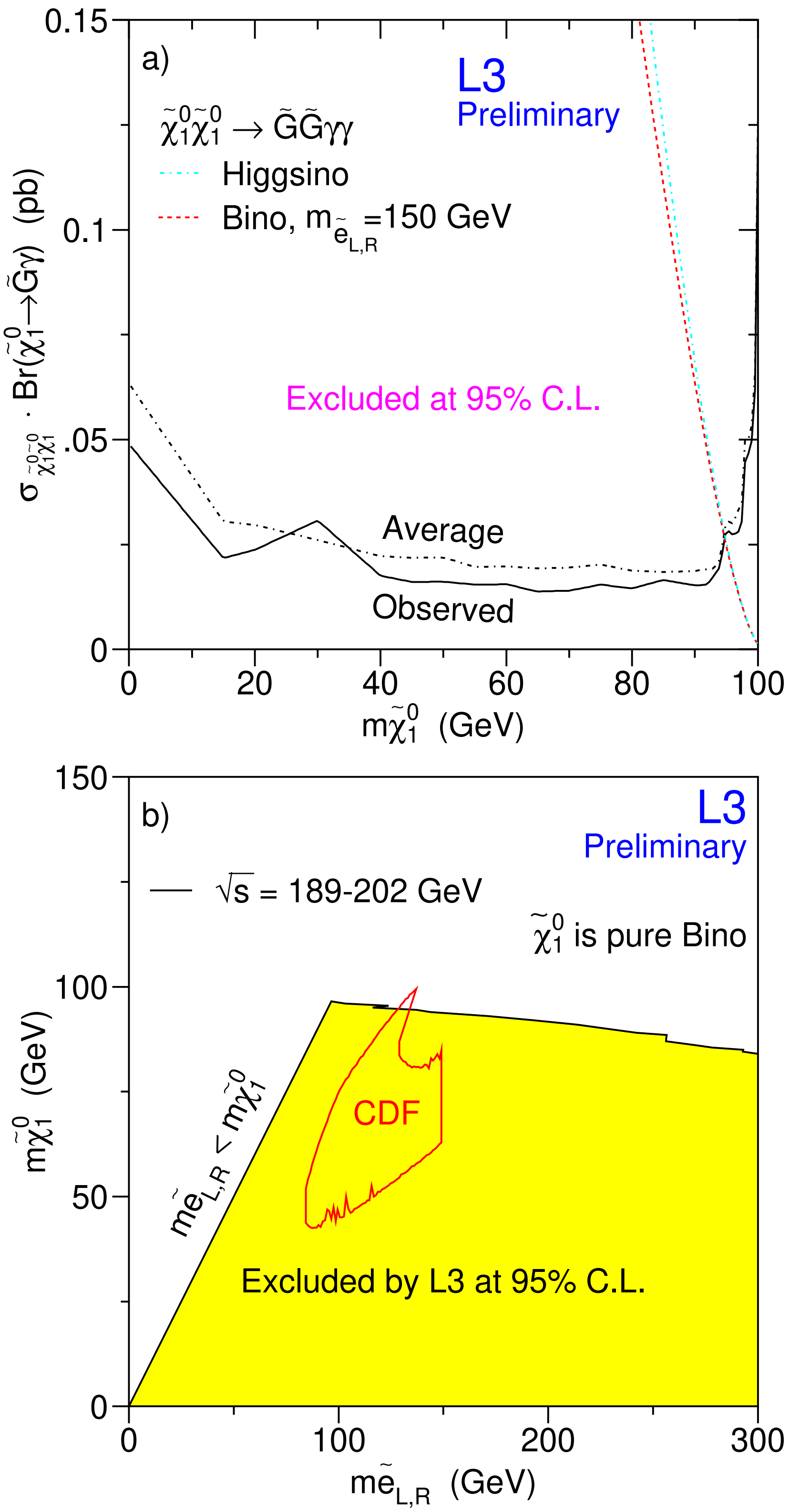


Figure 9: (a) Upper limit on the cross section for $e^+e^- \rightarrow \tilde{\chi}_1^0\tilde{\chi}_1^0 \rightarrow \tilde{G}\tilde{G}\gamma\gamma$ at $\sqrt{s} =$ 202 GeV. Data collected at lower centre-of-mass energies are included assuming the signal cross section to scale as $\beta/s$. Theoretical predictions for two extreme cases of $\tilde{\chi}_1^0$ composition are also shown. (b) Excluded region for a pure bino neutralino model compared to the region consistent with the supersymmetric interpretation of the CDF event in the scalar electron scenario [26].